The MICROSCOPE space mission to test the equivalence principle

Gilles Metris, Manuel Rodrigues, Joel Bergé

THE MICROSCOPE SPACE MISSION TO TEST THE EQUIVALENCE PRINCIPLE

G. MÉTRIS[1], M. RODRIGUES[2], J. BERGÉ[2]

[1] Université Côte d'Azur, Observatoire de la Côte d'Azur, CNRS, Géoazur - France - gilles.metris@oca.eu

[2] DPHY, ONERA, Université Paris Saclay - France

ABSTRACT. The MICROSCOPE mission tested the Weak Equivalence Principle (WEP) with an unprecedented precision of order 10^{-15}, two orders of magnitude better than the previous best lab experiments. While the WEP, the cornerstone of General Relativity (GR), does not sway, the decade-long problems faced by fundamental physics stay still: how can we unify GR with the Standard Model, and how can we explain the acceleration of the cosmological expansion? As most beyond-GR models predict a violation of the WEP, albeit at an unknown level, it remains critical to even better test the WEP. In this paper, we review the MICROSCOPE mission and give its final constraint on the WEP.

1. INTRODUCTION

The universality of free-fall (UFF) has been recognised since Galileo rolled objects down inclined planes and found that, locally, they all undergo the same gravitational acceleration: all objects within the same gravitational field fall at the same rate, independently of their mass and composition. With Newton's second law, the UFF can be restated as the proportionality between the gravitational mass m_G and the inertial mass m_I, with the same proportionality constant for all bodies: this is the usual definition of the weak equivalence principle (WEP). The Equivalence Principle, as generalised by Einstein, was the starting point to general relativity (GR).

GR describes gravitation as the simple spacetime's curvature, while recovering Newton's description of gravitation as a classical inverse-square law force in weak gravitational fields and for velocities small compared to the speed of light. As a highly predictive theory, it has so far successfully passed all experimental tests [1, 2]. Standing next to GR, the Standard Model (SM) was built from the realisation that the microscopic world is intrinsically quantum.

Although both GR and SM leave few doubts about their validity in their respective regimes, scientists have been faced with difficulties for decades. Firstly, the question of whether GR and the SM should and could be unified remains open: major theoretical endeavours delivered models such as string theory, but still fail to provide a coherent vision of the world. Secondly, the unexpected dark matter and dark energy make up most of the Universe's mass-energy budget.

The WEP has been tested for four centuries with increased precision [3–10]. The concept of a test in space emerged in the 1970s [11, 12], motivated by the quiet environment that space can provide and by the benefit of test periods much longer than on-ground experiments. In 1999, ONERA (Office National d'Etudes et de Recherches Aérospatiales) and OCA (Observatoire de la Côte d'Azur) proposed the MICROSCOPE mission (MICRO-Satellite à Compensation de traînée pour l'Observation du Principe d'Equivalence) to CNES.

MICROSCOPE was finally launched in 2016. After successfully dealing with unexpected anomalies [13], the mission provided two and a half years of useful data. In 2017, a first analysis based on only 7% of the eventual science data allowed us to verify the WEP at 2×10^{-14} sensitivity level [14, 15]. In 2022, the full data allowed us to improve that precision by one order of magni-

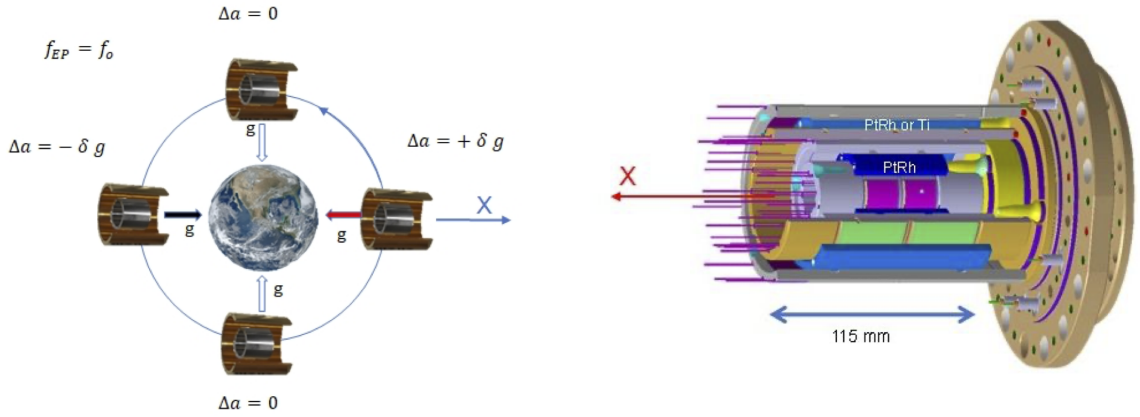

Figure 1: Experimental principle (left) and accelerometer core (right).

tude [16, 17]. In this paper, we first describe MICROSCOPE in Sect. 2. In Sect. 3, we describe the data processing and provide the upper bound provided by MICROSCOPE on the validity of the WEP.

2. MICROSCOPE MISSION OVERVIEW

2.1 WEP test experiment principle

The measurement relies on comparing the accelerations of two concentric bodies – cylinders in the case of MICROSCOPE – in orbit around the Earth. As shown in Fig. 1, the measurement is performed along the cylinders' X-axis, which is aligned with their main axis. In an inertial pointing configuration, it is pointing in the same direction of the Earth's gravity field vector once per orbit. In a perfect case, the difference of acceleration is proportional to the Eötvös parameter defined by the relative ratio of difference of gravitational-to-inertial masses m_{gj}/m_{ij} between two materials j:

$$\delta(2,1) = 2\frac{a_2 - a_1}{a_2 + a_1} = 2\frac{m_{g2}/m_{i2} - m_{g1}/m_{i1}}{m_{g2}/m_{i2} + m_{g1}/m_{i1}}, \tag{1}$$

where a_j are the acceleration undergone by the two bodies.

In MICROSCOPE, the test-masses are part of a double concentric accelerometer. The test-masses are finely controlled by electrostatic forces to be motionless with respect to the surrounding electrodes as illustrated in the right panel of Fig. 1. The forces applied by the set of electrodes are determined by the voltage applied on the test-mass and on each electrode [18]. The combination of these voltages with the geometry of the instrument defines the electrostatic forces and torques applied to each test-mass in order to counteract all the other effects that prevent the test-mass to stay motionless with respect to the satellite.

Thus, if a WEP violation exists, it can be detected as a signal with a well-known frequency (the orbital frequency $f_{\rm orb}$ in the case of Fig. 1) in the differential acceleration measured by the accelerometer (i.e., the difference of electrostatic force per unit mass between the two test masses). The measurement precision can be improved by rotating the satellite about the axis normal to the orbital plane. This increases the modulation frequency of the Earth's gravity vector projected onto the X-axis, to put it closer to the minimum of the instrumental noise. The WEP-violation frequency becomes $f_{\rm EP} = f_{\rm orb} + f_{\rm spin}$, with $f_{\rm spin}$ the rotation frequency of the satellite. Two spin frequencies have been used during the mission, leading to two test measurement data sets at $f_{\rm EP} \approx 0.9 \times 10^{-3}$ Hz and $f_{\rm EP} \approx 3.1 \times 10^{-3}$ Hz.

2.2 Payload

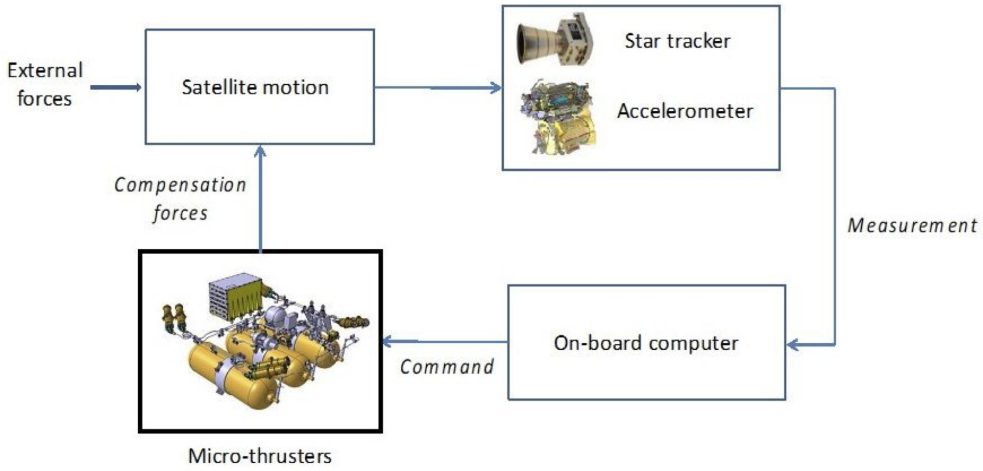

Figure 2: Satellite Drag-Free and Attitude Control System

The payload [18] is composed of two identical differential accelerometers also called sensor units (SUs) except for the test-mass material. Each SU have two concentric hollow cylindrical test-masses surrounded by electrodes engraved on gold-coated silica parts. Each SU is connected to a front-end electronics unit (FEEU) which delivers the voltages to the test-masses and electrodes and transmits the data to the interface control unit (ICU). Each ICU connected to the FEEU contains all the digital electronics and software to operate the test-mass control servo-loops and data conditioning for the satellite and then the ground telemetry. The SU and the FEEU are integrated in a thermal cocoon placed at the core of the satellite which offers a micro-Kelvin stability around the measurement frequencies.

The first SU, called SUREF, comprises two test-masses of the same material: PtRh10 platinum-rhodium alloy containing 90% by mass of Pt ($A = 195.1$, $Z = 78$) and 10% Rh ($A = 102.9$, $Z = 45$). SUREF is dedicated to experiment and accuracy verification (in orbit or on ground within the data processing) as it is supposed to give a null signal at f_{EP}. The second SU, called SUEP, comprises two test-masses of different material: the same PtRh10 alloy for the inner test-mass and an aeronautic titanium alloy (TA6V) for the outer test-mass with the atomic composition 90% of titanium ($A = 47.9$, $Z = 22$), 6% of aluminium ($A = 27.0$, $Z = 13$) and 4% of vanadium ($A = 50.9$, $Z = 23$). SUEP is dedicated to the WEP test.

Each test-mass defines a six-degree-of-freedom accelerometer. In order to operate in the most quiet environment and to get the most accurate orientation of the satellite, the accelerometer outputs are used by the satellite's drag-free and attitude control system (DFACS): it applies the necessary commands to the cold gas thrusters (Fig. 2). Atmospheric drag, Sun and Earth radiation forces, magnetic torques and all other disturbing sources are therefore compensated in order to nullify the common mode of one of the SU (i.e., either the mean acceleration of the two concentric test-masses or one of the acceleration output). The accelerometer's output or its internal servo-loop can be artificially biased at a particular frequency to stimulate the test-mass or the satellite (linear or angular motion) during calibration sessions.

2.3 Drag-free satellite

One of the challenges of the mission objectives is to make the satellite environment as quiet as possible for the payload to prevent any corruption of acceleration measurements.

The MICROSCOPE mission has been developed on the basis of scientific missions exploiting

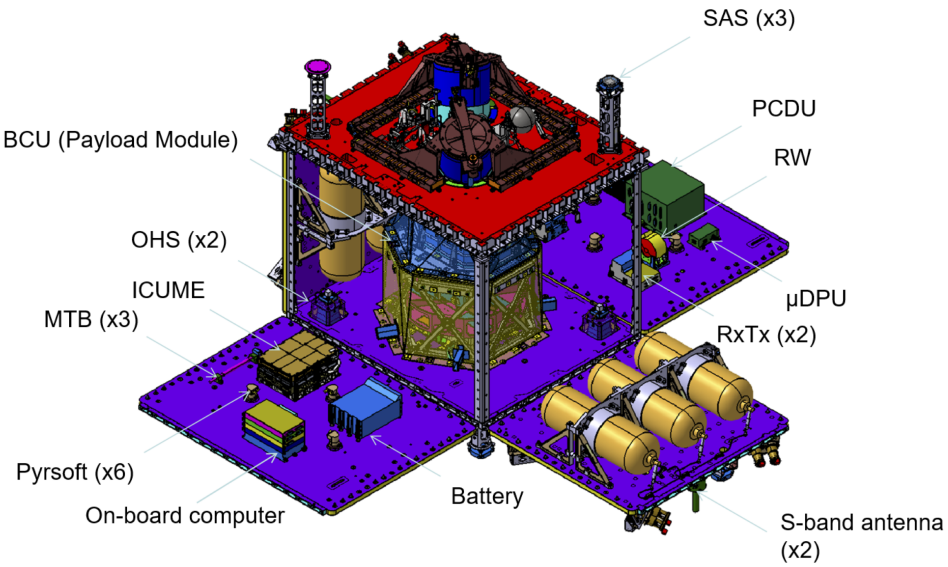

Figure 3: The cube forming the satellite is open in the picture, the instrument T-SAGE is at the center surrounded by the two 2×3 tanks of the cold gas propulsion system. Once closed the satellite cube measures $1.4\,\mathrm{m} \times 1\,\mathrm{m} \times 1.5\,\mathrm{m}$ and weighs about 300 kg.

the CNES MYRIADE microsatellite product line whose architecture comprises a platform with generic functional chains (energy, communication, computer, structure, etc.). Some adaptations and modifications were necessary to cope with the unusual performance requirements. Usually, the payloads of the MYRIADE satellites are located on the decoupled upper part of the platform but MICROSCOPE payload module has been accommodated at the center of the spacecraft where it could take advantage of a more stable thermal environment (Fig. 3).

The satellite thermal design has been optimised to offer the payload a tight temperature stability: the required stability around the WEP test frequency f_{EP} was set to 1 mK at the sensor unit interface and to 10 mK at the associated analog electronics interface. Active heaters did not operate during the science operations in order to avoid any interference with the payload measurements. Consequently, the thermal control on the satellite purely relied on passive methods: the dissipation of the electronic units was ensured by satellite external radiators. The in-orbit estimated thermal performance exceeded requirements and expectations. The payload was also shielded from the Earth and satellite magnetic field. In addition, the mechanical or electronic micro disturbances were minimized by a careful design and analysis to ensure an optimal environment: choice of multi-layer insulation (MLI) to minimize cracking, minimisation of current loops, study of thermoelastic deformations to estimate internal gravitational effects...

To counteract non-gravitational forces and torques, an active control of accelerations and attitude of the satellite was implemented through the DFACS (Fig. 2). The DFACS used the scientific instrument itself as main sensor for delivering the linear as well as the angular accelerations hybridized with the star tracker measurements. The control laws for acceleration and attitude estimated the total forces and torques to be applied on the satellite which were transformed into eight micro-thrust commands sent to the cold gas propulsion system placed on two opposite walls of the satellite (Fig. 3). Each of the eight pods of thrusters actually comprises two thrusters: one nominal and one redudant not operating but that could be switched on in case of failure

of the nominal. The DFACS in-orbit performances allowed to reduce the disturbances by 90 dB around f_{EP} leading to a controlled linear acceleration better than $3 \times 10^{-13}\,\mathrm{m\,s^{-2}}$, one order of magnitude better than expectation. The satellite attitude was controlled to better than 1 μrad at f_{EP} with an angular velocity stability better than $3 \times 10^{-10}\,\mathrm{rad\,s^{-1}}$ at f_{EP} in rotating mode, one order of magnitude better than expectation as well. The induced angular acceleration was controlled to better than $10^{-11}\,\mathrm{rad\,s^{-2}}$ at f_{EP}, limiting centrifugal effects due to the off-centring of the test-masses.

Besides, the DFACS was able to receive additional external sine signals at particular frequencies in order to calibrate the instrument (differential scale factor, test-mass alignments and off-centerings, coupling between axes, non-linearity). Particular sessions were also dedicated to thermal sensitivities thanks to dedicated heaters.

3. DATA PROCESSING AND RESULTS

3.1 Measurement equation

A single accelerometer (called inertial sensor) measures the difference of acceleration between the test-mass of the accelerometer and the center of mass of the satellite. A differential accelerometer yields the difference $\vec{\Gamma}^{(d)} = \vec{\Gamma}^{(1)} - \vec{\Gamma}^{(2)}$ of two such accelerations for two test-masses. The accelerometers are not perfect, in the sense that we look for very small signals and thus any little defect can make deviate from an ideal response: they have bias, scale factors departing from unity, non-zero coupling between axes [19]. Moreover, their orientation in the satellite, in space and with respect to the Earth's gravity field, is not perfectly known. That is why the measured differential acceleration $\vec{\Gamma}^{(d)}$ is not identical to the real one $\vec{\gamma}^{(d)}$, but is related to it as [19]:

$$\vec{\Gamma}^{(d)} = \vec{b_0}^{(d)} + \left[\mathbf{A}^{(c)}\right] \vec{\gamma}^{(d)} + 2\left[\mathbf{A}^{(d)}\right] \vec{\gamma}^{(c)} + \vec{n}^{(d)}, \tag{2}$$

where

- $\vec{b_0}^{(d)}$ is the difference of bias between the two inertial sensors;
- $\left[\mathbf{A}^{(c)}\right]$ is the common mode sensitivity matrix, close to the identity matrix, which includes scale factors, coupling between axes and global rotation common to the two sensors;
- $\left[\mathbf{A}^{(d)}\right]$ is the differential mode sensitivity matrix, very small, which takes into account the difference of characteristics of the two sensors;
- $\vec{\gamma}^{(c)}$ is the common mode acceleration which is mainly due to non-gravitational accelerations acting on the satellite and not on the enclosed test-masses; these non-gravitational accelerations include drag and radiation pressures and the thrust applied to the satellite which is servo-controlled in order to considerably reduce $\vec{\gamma}^{(c)}$ in the frequency band of interest;
- $\vec{n}^{(d)}$ is the (colored) noise.

In addition, couplings with angular accelerations and nonlinearities can also arise. These terms are not formally included in the above equation but specific measurement sessions have been dedicated to the identification of such effects and demonstrated that they are negligible [20].

The potential WEP-violation signal, $\delta(2,1)\vec{g}$, is included in $\vec{\gamma}^{(d)}$ which also contains the gravity gradient and the differential angular acceleration due to the small residual off-centring between the two test-masses [19]:

$$\vec{\gamma}^{(d)} = \delta(2,1)\vec{g}(O_{\mathrm{sat}}) + ([\mathrm{T}] - [\mathrm{In}])\vec{\Delta} + \vec{b_1}^{(d)}, \tag{3}$$

where

- $\vec{g}(O_{\text{sat}})$ is the gravity acceleration;
- [T] is the gravity gradient tensor;
- [In] is the gradient of inertia matrix;
- $\vec{\Delta}$ is the off-centring vector from the center of test-mass (1) to the center of test-mass (2);
- $\vec{b_1}^{(d)}$ contains the differences between the other small (mainly non gravitational) perturbations acting on the two test-masses.

Only the axis of the cylindrical test-masses, called X, which is much more precise than the other axes is used to estimate the EP signal. Therefore Eq. (2) has to be projected onto the X-axis. This leads to numerous terms [19] but the following considerations lead to simplifications for the reader's convenience:

- the more impacting components of the sensitivity matrix are estimated thanks to dedicated calibrations [21];
- the projection of the common mode is corrected thanks to the calibration of $\left[\mathbf{A}^{(d)}\right]$ and the measurement of $\vec{\gamma}^{(c)}$ (which is roughly assimilated to $\vec{\Gamma}^{(c)}$);
- the effect of the angular acceleration (anti-symmetric part of matrix [In]) is neglected (in practice we can correct for it but we have verified that this has no impact at the f_{EP} frequency thanks to the very good stability of the attitude control);
- small terms as the effect of the out-of-orbital-plane component of the off-centring are corrected thanks to dedicated calibrations;
- the tiny impact of the bias at the f_{EP} frequency is included in the evaluation of the systematic effects.

The remaining model used to analyse the measurements along the X-axis reads

$$\Gamma^{(d)}_{x,\text{corr}} = \sum_{j=0}^{3} \alpha_j (t - t_0)^j + \delta_x g_x + \delta_z g_z + \Delta'_x S_{xx} + \Delta'_z S_{xz} + n_x^{(d)}, \tag{4}$$

where

- $\delta_x \approx A^{(c)}_{(1,1)} \delta(2,1)$ ($A^{(c)}_{(1,1)}$ being the scale factor along X) is very close to the Eötvös ratio;
- δ_z, a small fraction of $\delta(2,1)$, is in principle too small to be estimated but is included in the model to check the absence of anomaly;
- S_{xx} and S_{xz} are components of the matrix [S] which is the symmetric part of [T] $-$ [In];
- Δ'_x (close to Δ_x) and Δ'_z (close to Δ_z) are "effective" components of the off-centring taking into account the sensitivity matrix;
- $\sum_{j=0}^{3} \alpha_j (t - t_0)^j$ is an empirical polynomial term aiming to absorb the effect of the bias and its slow drift (mainly due to thermal effects).

3.2 Results

The final results of the MICROSCOPE mission are based on eighteen sessions for SUEP and nine sessions for SUREF [17]. A few sessions were discarded because of non-linearities at the

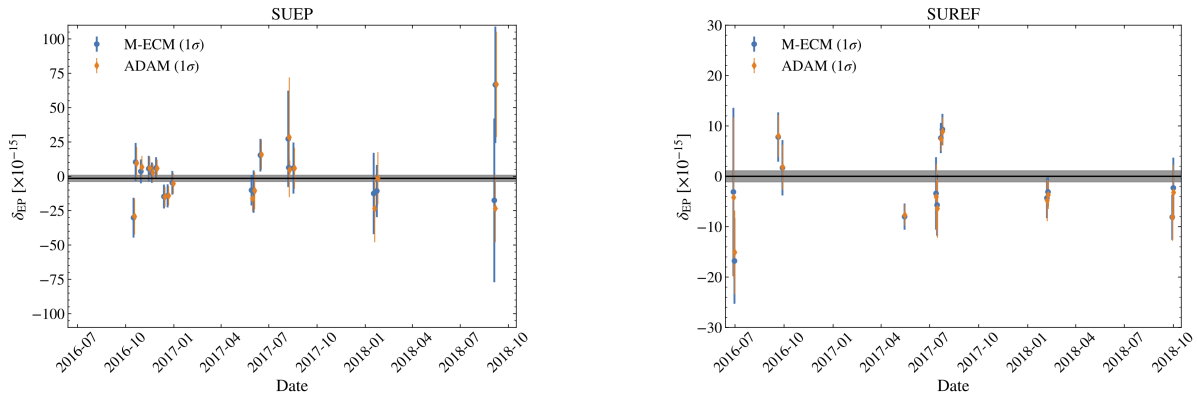

Figure 4: Eötvös parameter estimates for each SUEP (left panel) and SUREF (right panel) session and their 68% confidence error bars. Blue circles show M-ECM's estimates and orange ones Adam's.

beginning of the mission (before the control loop's electronics was upgraded) and a few others were discarded because of rare anomalies.

Beside EP-test sessions, in-flight calibration sessions were designed to estimate parameters so that the (perturbing) signals they source have a favourable signal-to-noise ratio (each session being dedicated to one or two parameters). We use the fact that parameters are almost independent to simplify and better control the estimation process with an iterative method based on the Adam (Accelerometric Data Analysis for MICROSCOPE) code to estimate parameters in the frequency domain [22].

In practice, instrumental defects are parameterized by the $\overrightarrow{b}_1^{(d)}$ and $\overrightarrow{\Delta}$ vectors, as well as the $\left[A^{(d)}\right]$ and $\left[A^{(c)}\right]$ matrices in Eq. (4), with only some of their components impacting the projected acceleration [19, 21]. The estimation of Δ'_x and Δ'_z uses their couplings with the Earth gravity gradient, whose strong spectral line at $2f_{\mathrm{EP}}$ allows for a direct determination in science data based on an accurate Earth gravity model. Dedicated five-orbit sessions were used to measure Δ'_y, where the satellite was oscillated about the z-axis at a frequency f_{cal} to create a measurable signal driven by Δ'_y. The elements of the first row of the $[A^{(d)}]$ matrix a_{d1i} were measured by shaking the satellite at frequency f_{cal} along each axis (x to measure a_{d11}, y for a_{d12} and z for a_{d13}) in order to drive a measurable signal dependent on those parameters. The a_{d11} sessions also allowed for a measurement of the differential quadratic factor $K_{2d,xx}$ at $2f_{\mathrm{cal}}$. Once the above iterative process converges, the Eötvös parameter is estimated on calibrated data following Eq. (4).

Two different methods have been developed for theses estimations. The first one relies on a modified expectation-maximization algorithm (M-ECM), an iterative process which estimates the model parameters together with the missing data [23] until a convergence criterion is reached. The second method, Adam (Accelerometric Data Analysis for MICROSCOPE) estimates the parameters by means of a weighted least square regression in the frequency domain [22].

In a first step, the Eötvös parameter was estimated separately on each session. The results are depicted on Fig. 4.

A meticulous analysis of systematic errors, dominated by thermal effects, has been conducted based on numerous specific sessions dedicated to quantifying these effects. This led to a maximum systematic error for each session [21].

In a second step, measurements from all sessions were accumulated for a global estimate of the Eötvös parameter. The final MICROSCOPE's constraint on the validity of the WEP is [16, 17]

$$\delta(\mathrm{Ti},\mathrm{Pt}) = [-1.5 \pm 2.3\ (\mathrm{stat}) \pm 1.5\ (\mathrm{syst})] \times 10^{-15}, \tag{5}$$

where the statistical error is given at 1σ.

The reference instrument provided a null result, $\delta(\mathrm{Pt},\mathrm{Pt}) = [0.0 \pm 1.1\ (\mathrm{stat}) \pm 2.3\ (\mathrm{syst})] \times 10^{-15}$, showing no sign of unaccounted systematic errors in Eq. (5). As expected from its higher sensitivity, SUREF's result has a smaller statistical error than SUEP's. On the opposite, it has higher systematic errors (dominated by thermal effects), since they were estimated with less optimal sessions than SUEP's ones [21].

4. CONCLUSION

The MICROSCOPE mission has delivered its final measurement on October 2018. Since then, the science team has put a lot of effort into verifying all the data. The estimation of systematic errors have been improved with respect the first results obtained in 2017 to a few 10^{-15} in Eötvös parameter units. This allowed for an unprecedented precision on the test of the WEP.

With the lessons learned from the MICROSCOPE mission, we identified key parts of the instrument, satellite and operations that can be improved to beat MICROSCOPE's precision on the test of the WEP by two orders of magnitude. A space mission, as similar as possible to MICROSCOPE (which we tentatively call MICROSCOPE 2) could be designed with only almost off-the-shelf technology. Indeed, most improvements have already been shown to work in space, while others, more demanding, are not compulsory for the success of such as mission. We could thus expect a follow-up mission to MICROSCOPE to fly in the next few decades, on a low enough budget, but with high science outcomes about GR's validity and about ultra-light dark matter.

MICROSCOPE data are available at https://cmsm-ds.onera.fr.

Acknowledgments

The authors express their gratitude to all the different services involved in the mission partners and in particular the French space agency CNES in charge of the satellite. This work is based on observations made with the T-SAGE instrument, installed on the CNES-ESA-ONERA-CNRS-OCA-DLR-ZARM MICROSCOPE mission. ONERA authors' work is financially supported by CNES and ONERA fundings. Authors from Observatoire de la Côte d'Azur (OCA) have been supported by OCA, the French National Center for Scientific Research (CNRS), and CNES. ZARM authors' work is supported by the German Space Agency DLR, with funds of the BMWi (FKZ 50 OY 1305 and FKZ 50 LZ 1802) and by the Deutsche Forschungsgemeinschaft DFG (LA 905/12-1). The authors would like to thank the Physikalisch-Technische Bundesanstalt institute in Braunschweig, Germany, for their contribution to the development of the test-masses with funds from CNES and DLR.

5. REFERENCES

[1] Will, C. M.,2014,"The Confrontation between General Relativity and Experiment", Living Reviews in Relativity, 17, 4.

[2] Ishak, M., 2019, "Testing general relativity in cosmology", Living Reviews in Relativity, 22, 1.

[3] Eötvös, L., Pekár, D., Fekete, E., 1922, "Beiträge zum Gesetz der Proportionalität von Trägheit and Gravität", Ann. Phys., 68, p. 11.

[4] Bessel, F. W., 1832, "Versuche über die Kraft mit welcher die Erde Körper von verschiedene Beschaffendheit anzieht", Ann. Phys. Chem. (Poggendorf), 25, 401-17.

[5] Roll, P. G., Krotkov, R., Dicke, R.H., 1964, "The equivalence of inertial and passive gravitational mass, Annals Phys., 26, p. 442-517.

[6] Braginskii, V. B., Panov V. I., 1971, "Verification of equivalence of inertial and gravitational masses, Zh. Eksp. Teor. Fiz., 61, 873-879.

[7] Schlamminger, S., Choi, K.-Y., Wagner, T. A., Gundlach, J. H., Adelberger, E. G., 2008, "Test of the Equivalence Principle Using a Rotating Torsion Balance", Physical Review Letters, 100, 4, 041101.

[8] Wagner, T. A., Schlamminger, S., Gundlach, J. H., Adelberger, E. G., 2012, "Torsion-balance tests of the weak equivalence principle", Class. Quant. Grav., 29, 18, p. 184002.

[9] Williams, J. G., Turyshev, S. G., Boggs, D. H., 2012, "Lunar laser ranging tests of the equivalence principle", Classical and Quantum Gravity, 29, 18, p. 184004.

[10] Viswanathan, V., Fienga, A., Minazzoli, O., Bernus, L., Laskar, J., Gastineau, M., 2018, "The new lunar ephemeris INPOP17a and its application to fundamental physics", MNRAS, 476, p. 1877-1888.

[11] Chapman, P. K. and Hanson, A. J., 1970, "An Eötvös Experiment in Earth Orbit, Davies, R. W. (Ed.)", Proc. Conf. on Experimental Tests of Gravitation TheoriesJPL TM, 33-499, p. 228.

[12] Everitt, C. W. F., Damour, T., Nordtvedt, K., Reinhard, R., 2003, "Historical perspective on testing the Equivalence Principle", Advances in Space Research, 32, 1297–1300.

[13] Rodrigues, M. et al., 2022, "MICROSCOPE Mission scenario, ground segment and data processing", Classical and Quantum Gravity, 39, 204004.

[14] Touboul, P. et al., 2017, "MICROSCOPE Mission: First Results of a Space Test of the Equivalence Principle", Physical Review Letters, 119, 231101.

[15] Touboul, P. et al, 2019, "Space test of the equivalence principle: first results of the MICROSCOPE mission", Classical and Quantum Gravity, 36, 22.

[16] Touboul, P. et al, 2022, "MICROSCOPE Mission: Final Results of the Test of the Equivalence Principle", Physical Review Letters, 129, 121102.

[17] Touboul, P. et al, 2022, "Result of the MICROSCOPE weak equivalence principle test", Classical and Quantum Gravity, 39, 204009.

[18] Liorzou, F. et al., 2022, "MICROSCOPE instrument description and validation.", Classical and Quantum Gravity, 39, 204002.

[19] Touboul, P. et al, 2022, "MICROSCOPE mission analysis, requirements and expected performance", Classical and Quantum Gravity, 39, 204001.

[20] Chhun, R. et al, 2022, "MICROSCOPE instrument in-flight characterization", Classical and Quantum Gravity, 39, 204005.

[21] Rodrigues, M. et al, 2022, "MICROSCOPE: systematic errors", Classical and Quantum Gravit, 39, 204006.

[22] Bergé, J. et al, 2022, "MICROSCOPE mission: data analysis principle", Classical and Quantum Gravity, 39, 204007.

[23] Baghi, A., Métris, G., Bergé, J., Christophe, B., Touboul, P., Rodrigues, M., 2016, " Gaussian regression and power spectral density estimation with missing data: The MICROSCOPE space mission as a case study", Physical Review D, 93, 12, p. 122-007.